European Journal of Radiology Open 8 (2021) 100378

Contents lists available at ScienceDirect

European Journal of Radiology Open

journal homepage: www.elsevier.com/locate/ejro

Preliminary study of multiple b-value diffusion-weighted images and T1 post enhancement magnetic resonance imaging images fusion with Laplacian Re-decomposition (LRD) medical fusion algorithm for glioma grading

Amir Khorasani [a], Mohamad Bagher Tavakoli [a,*], Masih Saboori [b], Milad Jalilian [a]

[a] Department of Medical Physics, School of Medicine, Isfahan University of Medical Sciences, Isfahan, Iran
[b] Department of Neurosurgery, School of Medicine, Isfahan University of Medical Sciences, Isfahan, Iran

HIGHLIGHTS

- LRD medical image fusion algorithm can be used for glioma grading.
- We can use the LRD fusion algorithm with MRI image for glioma grading.
- Fusing of DWI (b50) and T_1 enhancement (T_1Gd) by LRD, have highest diagnostic value for glioma grading.

ARTICLE INFO

Keywords:
Fusion algorithm
Glioma
Grade
Magnetic resonance imaging
Laplacian Re-decomposition
Diffusion-weighted images

ABSTRACT

Background: Grade of brain tumor is thought to be the most significant and crucial component in treatment management. Recent development in medical imaging techniques have led to the introduce non-invasive methods for brain tumor grading such as different magnetic resonance imaging (MRI) protocols. Combination of different MRI protocols with fusion algorithms for tumor grading is used to increase diagnostic improvement. This paper investigated the efficiency of the Laplacian Re-decomposition (LRD) fusion algorithms for glioma grading.

Procedures: In this study, 69 patients were examined with MRI. The T1 post enhancement (T1Gd) and diffusion-weighted images (DWI) were obtained. To evaluated LRD performance for glioma grading, we compared the parameters of the receiver operating characteristic (ROC) curves.

Findings: We found that the average Relative Signal Contrast (RSC) for high-grade gliomas is greater than RSCs for low-grade gliomas in T1Gd images and all fused images. No significant difference in RSCs of DWI images was observed between low-grade and high-grade gliomas. However, a significant RSCs difference was detected between grade III and IV in the T1Gd, b50, and all fussed images.

Conclusions: This research suggests that T1Gd images are an appropriate imaging protocol for separating low-grade and high-grade gliomas. According to the findings of this study, we may use the LRD fusion algorithm to increase the diagnostic value of T1Gd and DWI picture for grades III and IV glioma distinction. In conclusion, this article has emphasized the significance of the LRD fusion algorithm as a tool for differentiating grade III and IV gliomas.

Abbreviations: LRD, Laplacian Re-decomposition; MRI, magnetic resonance imaging; T1Gd, T1 post enhancement; BOLD, blood oxygen level dependent imaging; CBV, Cerebral Blood Volume; GBM, glioblastomas; ADC, apparent diffusion coefficient; ROC, receiver operating characteristic curve; RSC, Relative Signal Contrast; AUC, Aera Under Curve; DWI, Diffusion-weighted imaging; SCE, Susceptibility contrast enhancement; DCE, Dynamic contrast enhancement; MRS, Magnetic resonance spectroscopy; MST, Multi-scale transform; TR, repetition time; TE, time of echo; TI, time of inversion; FA, flip angle; PACS, PACS picture archiving and communication system; GDIE, Gradient Domain Image Enhancement; MLD, Maximum Local Difference; LP, Laplacian Pyramid; DGR, Decision Graph Re-decomposition; LEM, Local Energy Maximum; OD, overlapping domain; NOD, Non-overlapping domain; IRS, Inverse Re-decomposition Scheme; ROI, regions of interest.

* Corresponding author at: Department of Medical Physics, School of Medicine, Isfahan University of Medical Sciences, Isfahan, 81746-73461, Iran.
E-mail address: mbtavakoli@mui.ac.ir (M.B. Tavakoli).

https://doi.org/10.1016/j.ejro.2021.100378
Received 9 August 2021; Received in revised form 20 September 2021; Accepted 26 September 2021

1. Introduction

Gliomas are the most common type of primary neoplasms of the brain in adults [1,2]. Based on the histopathological assessment of the tumor, gliomas can be classified into low-grade (grade I and II) and high-grade (grade III and IV) [2]. The main treatment options for brain tumors are surgery, radiation therapy, chemotherapy, or a combination of these treatments [3]. Tumor grade is believed to be the most essential and critical factor for treatment management [2]. The current benchmark for brain tumor grading are common tumor morphologic observations and histopathologic detection, but these methods have limitations of significant intra-observer difference, error in tissue sampling during the biopsy, and invasive process [4,5].

Development in medical imaging techniques has led to the proposed and investigated non-invasive methods for brain tumor grading. Advanced MRI imaging and functional imaging techniques such as diffusion-weighted imaging (DWI), dynamic susceptibility contrast enhancement imaging (DSC), blood oxygen level dependent imaging (BOLD), etc., prepare physiologic data that supplement the anatomic data acquired from standard MRI imaging modality [6–9]. Much works on the potential of parametric MRI imaging such as DWI, dynamic contrast enhancement (DCE), magnetic resonance spectroscopy (MRS), etc., have been carried out to determine the diagnostic value of MRI imaging protocols for tumor grading. Advanced MRI imaging and functional imaging techniques provided us the different physiologic information of the interested tissue with different accuracy. DWI measures the tissue cellularity by assuming that the water molecule's diffusivity within the extracellular part is inversely related to the intracellular space content and attenuation of water molecules in the tissue [10]. Because of decreased water diffusivity, the apparent diffusion coefficient (ADC) of DWI images decreases as tumor cellularity and grade increase. [9–11]. DSC enables the non-invasive analysis of tumor vascularity and angiogenesis. [6–9,12]. Because greater vascularity correlates to a higher tumor grade, the maximum tumor Cerebral Blood Volume (CBV) tends to increase with the astrocytoma grade [6,9,10].

Most previous works have only focused on tumor grading with single MRI image protocols [13–19]. A crucial issue of brain tumor grading with MRI images is the low accuracy of the traditional MRI methods. Few researchers have addressed the issue of the combination of different MRI protocols for tumor grading [20–22]. Hilario and co-workers [21] estimated the diagnostic accuracy of a combination of ADC and rCBV data for glioma grading. In [20] the authors investigated the usefulness of ADC and DCE-MRI parameters as predictive parameters for distinguishing between benign and malignant prostate lesions. Although MRI protocols such as DCE, DSC, BOLD, etc., are interesting, they do not become commercially available in all imaging departments and also need a high-specialist physician for image reports [23–25]. With this in mind, we tried to use conventional and widely available MRI imaging protocols such as regular T1 post-contrast enhancement (T1Gd) images and DWI images with multiple b-values in the current study.

One of the main different image data combination issues is the medical image fusion task. Image fusion is a popular technique for combining images from different imaging modalities or protocols, with the fused results retaining both image information [26]. In general, image fusion approaches are divided into two categories: spatial and transform domain methods. [27,28]. Transform domain-based methods are commonly used in medical image fusion [29,30].

In contrast to spatial domain techniques, transform domain methods first transform source images into specific coefficients. The coefficients are then fused, and by inversely transforming all of the fused coefficients, the fused image is reconstructed. Multi-scale transform (MST) and Sparse representation approaches have recently emerged as the most widely used image fusion techniques. The MST-based algorithm is a frequency domain approach use for image processing in medical imaging. Using a transform, MST-based algorithm separates source images into high and low-frequency sub-images and then produces separate fusion rules for the high and low-frequency sub-images to reconstruct the final fused image. One of the MST-based algorithm which used for medical image fusion, was Laplacian Re-decomposition (LRD) fusion algorithms.

We have designed an innovative solution for improving brain tumor grading accuracy with regular MRI images. The aim of this study is to evaluate the usefulness of LRD image fusion algorithm for brain tumor grading with DWI and T1 enhanced images of MRI and improve the grading accuracy for brain tumors with the fusion of conventional MRI images.

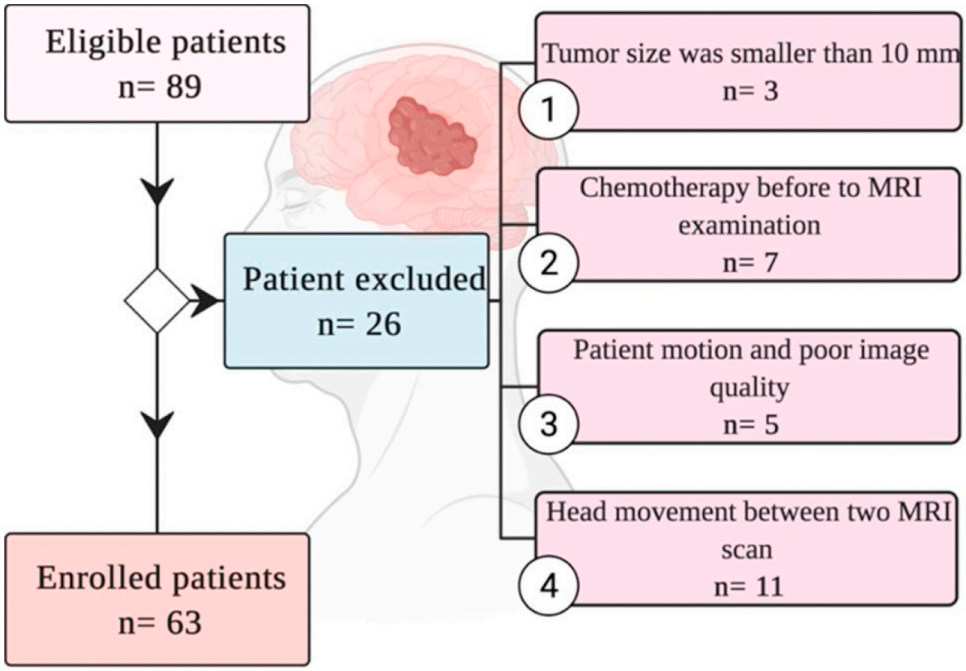

Fig. 1. Flow chart of the study population.

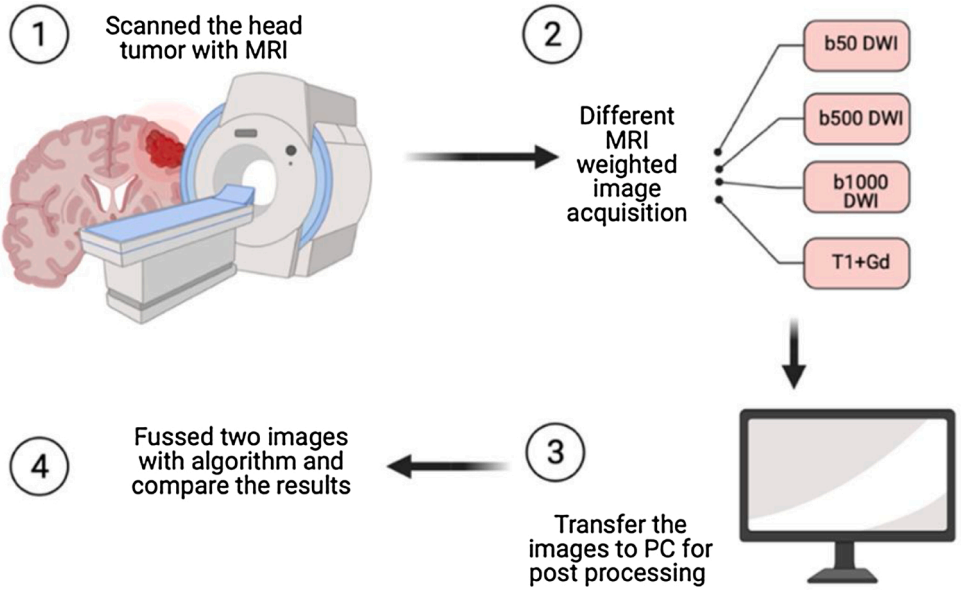

Fig. 2. Study design and steps.

2. Material and methods

2.1. Patient

This study included 89 patients with histologically confirmed gliomas by surgical resection who underwent magnetic resonance examination between April 2020 and February 2021. One experienced neuropathologist examined the tumor specimens according to the WHO 2016 classification [31].

Of these patients, 69 of them (36 men, 33 women; mean age 48 years; range [19 85] years), 16 low-grade gliomas (included 16 WHO grade II), and 53 high-grade gliomas (included 10 WHO grade III gliomas and 43 WHO grade IV glioblastomas (GBMs)) were included under the following criteria in this study: (1) histopathology confirmation of the gliomas; (2) lesion equal to or greater than 10 mm;(3) no radiotherapy or chemotherapy performed before the magnetic resonance imaging (MRI) examination; (4) adequate image quality (without patient motion or susceptibility artifact). Exclusion criteria were (1) patient motion or inadequate image quality; (2) lesion that was smaller than 10 mm; (3) allergy to gadolinium-based contrast agent; (4) chemotherapy performed before MRI examination. So, a total of 69 gliomas patients were analyzed in this study. Fig. 1 shows a flow chart of the study population. Before the MRI scan, all the patients provided informed consent, and the local research ethics committee has approved the study.

2.2. MRI imaging

MRI scan was performed with a 1.5 T scanner (GE MRI signa explorer 1.5 T) with a 16 channel head coil. We performed the following sequences: a 3-plane localizer sequence, axial T_1 pre-contrast (TR = 400 ms, TE = 10 ms, FA = 90, Slice thickness = 5 mm, and spacing = 5 mm) and post-contrast (TR = 6.1 ms, TE = 2.2 ms, TI = 20 ms, FA = 12, Slice thickness = 5 mm, and spacing = 5 mm), DWI imaging, and T_2 weighted images.

Echo-planar DWI images in the axial plane were acquired before administration of contrast media by using the following parameters: TR

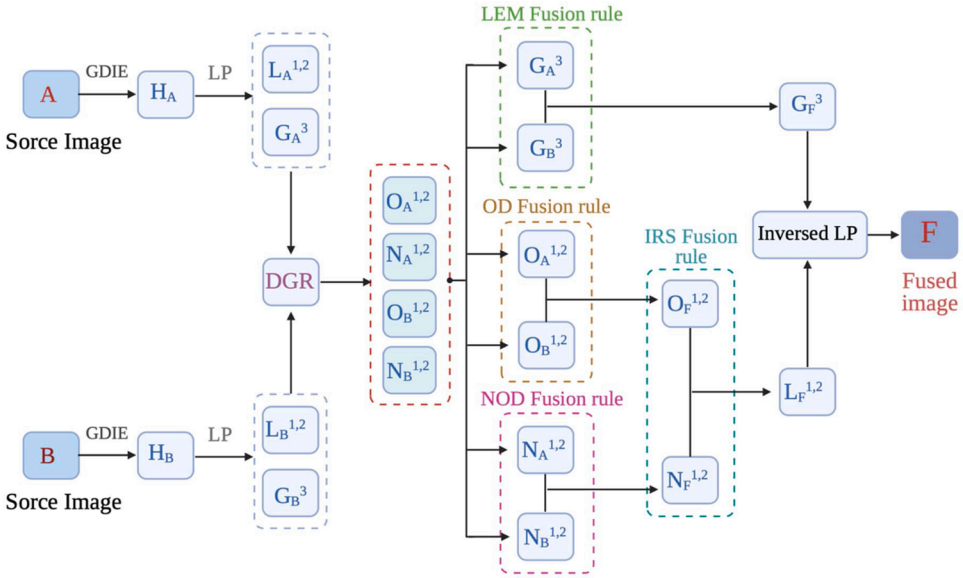

Fig. 3. Laplacian Re-decomposition (LRD) algorithm for medical image fusion includes several steps.
H_A and H_B: enhancement images, L_A and L_B: High-frequency sub-band images, G_A and G_B: Low-frequency sub-band images, O_A and O_B: overlapping domain images, N_A and N_B: Non-overlapping domain images, O_F: overlapping domain fusion images, N_F: Non-overlapping domain fusion images, G_F: low-frequency sub-band fusion images, L_F: high-frequency sub-band fusion images.

= 5268 ms, TE = 113.2 ms, FA = 90, Slice thickness = 5 mm, and spacing = 5 mm with b-values = 50, 500, 1000.

When b0 is used, bloods appear abnormally bright in DWI images and decrease the diagnostic value of the image. By raising the starting b-value to 50, providing a clear visualization of the tumor image and increasing the DWI image's diagnostic value.

2.3. Image fusion

The patient images were transferred from the picture archiving and communication system (PACS) to a personal computer (PC) (Fig. 2). In order to decrease the fusion time, all images were resized to 256*256. Fusion algorithm was performed using MATLAB 2019a Mathworks. The fusion algorithm used in this study is practically the same as the one proposed by Li et al. [26]. We chose this medical image fusion algorithm to better quantitatively and qualitatively than the other popular medical image fusion methods [26,32,33].

Briefly, the Laplacian Re-decomposition (LRD) algorithm for medical image fusion includes several steps (Fig. 3). In the LRD, we first used Gradient Domain Image Enhancement (GDIE) to produce Enhancement images (H_A and H_B) of each source image. In the next stage, Low-frequency (G_A and G_B) and High-frequency sub-band images (L_A and L_B) were created by using Laplacian pyramid transform (LP) from Enhancement images. Then with Decision Graph Re-decomposition (DGR), Overlapping domain (O_A and O_B), and non-overlapping domain (N_A and N_B), images were created. Finally, with local energy maximum (LEM) fusion rule, overlapping domain (OD) fusion rule, non-overlapping domain (NOD) fusion rule, inverse re-decomposition scheme (IRS) fusion rule, and inversed LP, the fused image was reconstructed. More details of this medical fusion algorithm are in [26].

2.4. Data evaluation

For each patient, the images in which the tumor size was the largest was selected as the image for data evaluation. In order to determine the image contrast, the mean signal intensity of two circular regions of interest (ROI) was calculated. ROIs were manually drawn by a radiologist in the T1 images with gadolinium injection (T1Gd) with the ImageJ software. These ROIs were located in: (1) in the white matter (WM) and (2) ROI region, which are enhancing tumor region (ER) on T1Gd for high-grade gliomas and high-signal intensity region on T2-weighted images for low-grade gliomas because on low-grade tumors the enhancement in T1Gd is scarce. ROIs drawn on T1Gd and T2 were transferred to co-aligned DWI images (b50, b500, and b1000) and fused images (T1Gd + b50, T1Gd + b500, and T1Gd + b1000). Three ROIs were sampled and averaged for each region to improve the comparison's power.

Then, Relative Signal Contrast (RSC) was calculated by:

$$RSC_{ROI} = \frac{\mu_{ROI} - \mu_{WM}}{\mu_{WM}}$$

Where, μ_{ROI} is the mean signal intensity of the ROI, and μ_{WM} is the mean signal intensity of the white matter as the mean background values in each picture. Seven RSC were calculated, RSC_{T1Gd}, RSC_{b50}, RSC_{b500}, RSC_{b1000}, $RSC_{T1Gd+b50}$, $RSC_{T1Gd+b500}$, $RSC_{T1Gd+b1000}$, and evaluated for brain tumor grading.

2.5. Statistical analysis

All statistical analysis was carried out using SPSS 26.0 software (IBM Corp. Armonk, NY, USA). Through the use of the Kolmogorov-Smirnov test, we were able to assess the normality distribution of parameters. Mean signal value and RSCs in the ROIs were compared between high-grade and low-grade groups with the two-tailed unpaired student's *t*-test. Also Exact Fisher test used for evaluation of the sex and age relationship with the tumor grade. The P-values of less than 0.05 were indicated to be statistically significant. A receiver operating characteristic (ROC) curve was chosen because it is one of the most practical ways to determine the cutoff values for differentiating high and low-grade gliomas with the best combination of sensitivity and specificity. The area under the curve (AUC) was calculated with the cut-off value set the maximum Youden index.

Table 1
characteristics of patient with low-grade and high-grade gliomas.

		Low-grade II	High-grade		P-value
			III	IV	
Number of patients		16 (19.11 %)	10 (14.71 %)	43 (66.18 %)	–
Mean age (years)		44.131 ± 16.59	51.88 ± 14.95		0.081
Sex	Man	7	29		0.57
	Woman	9	24		

3. Results

The study consisted of 16 low-grade (19.11 %) and 53 high-grade (80.87 %) gliomas. Among high-grade gliomas, 18.86 % were diagnosed as grade III and 81.14 % as grade IV. The histopathologic diagnoses are presented in Table 1. We did not find a significant difference in sex and ages between low-grade and high-grade gliomas (Table 1 and Fig. 4(a), 4(b)).

There was no significant difference in mean signal intensity values of normal-appearing white matter between the low-grade and high-grade gliomas (P-value >0.05). In Fig. 5, we show LRD fusion algorithm result on a patient with grade IV gliomas. Fig. 6 presents the some fused T1Gd and b50 images obtained from the LRD medical fusion algorithm for different glioma grade.

The average RSCs for low-grade and high-grade gliomas were shown in Table 2. In the fused images, the average RSCs in high-grade gliomas are greater than low-grade gliomas. No significant difference in RSCs of DWI images (b50, b500, b1000) was observed between low-grade and high-grade gliomas.

According to the LRD fusion algorithm results, there was a significant RSCs difference between grade III and IV in the T1Gd, b50, and all fussed (T1Gd + b50, T1Gd + b500, T1Gd + b1000) images (Fig. 7). However, the analysis did not show any significant differences between RSCs of b500 and b1000 images in grade III and IV gliomas groups (Fig. 7).

According to the ROC curve (Fig. 8) and (Table 3), the RSC cutoff value of 0.6826 in T1Gd + b50 images showed the highest sensitivity, specificity, and AUC in the differentiation of grade IV gliomas from grade III gliomas. Table 3 represents the cutoff value, AUC, sensitivity, specificity, and maximum Youden index for different RSCs in different images for discrimination of grade III and IV gliomas. The AUC to grade III and IV differentiation was 0.869 and 0.651 by using the T1Gd and b1000 images, respectively. Image fusion of T1Gd and b1000 images increased the AUC to 0.957 (47 % improvement toward b1000 images and 10.12 % improvement toward T1Gd images) (Table 3) to grade III and IV gliomas differentiation.

During ROC analysis of low-grade and high-grade differentiation (Fig. 9), RSCs of T1Gd images had greater AUC, sensitivity, and specificity than other RSCs of different images and fused images. Image fusion had increased the diagnostic performance of DWI (b50, b500, b1000) images for low-grade and high-grade discrimination (Fig. 9).

4. Discussion

Accurate grading of gliomas is one of the most essential factors for gliomas treatment decision [2]. Despite its invasiveness and shortcoming, biopsies and sampling have been widely and clinically used for gliomas grading [34]. Current solutions to a non-invasive and accurate method for glioma grading are using different imaging modalities such

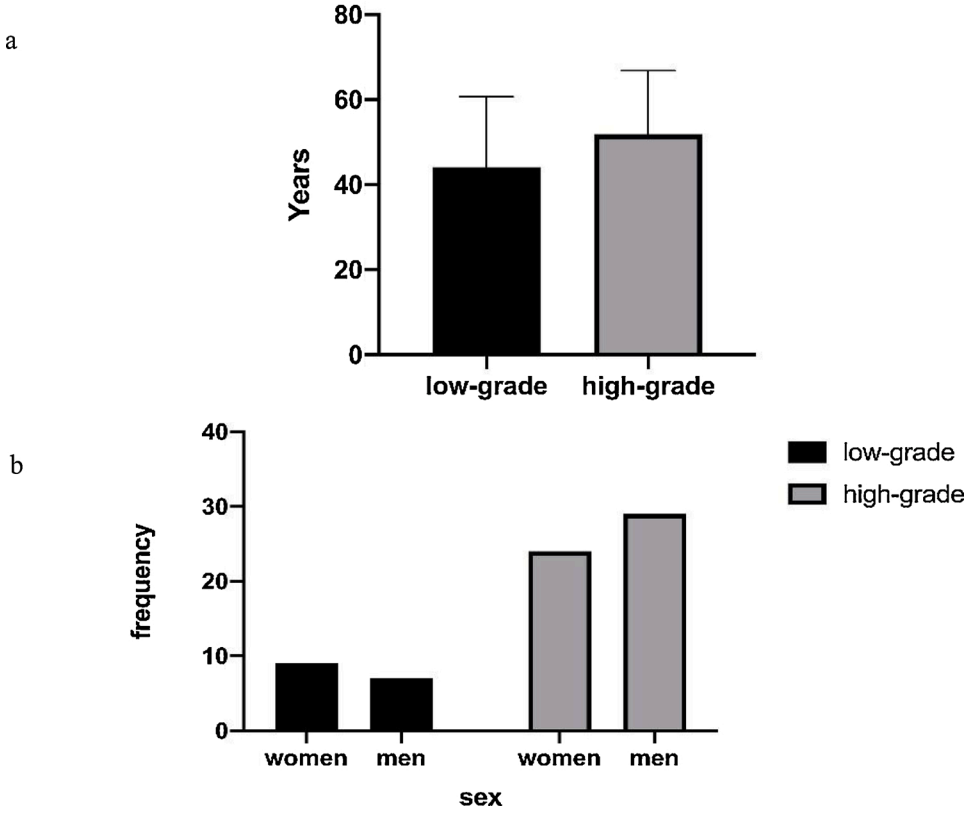

Fig. 4. years (a) and sex (b) of the patient in low-grade and high-grade groups.

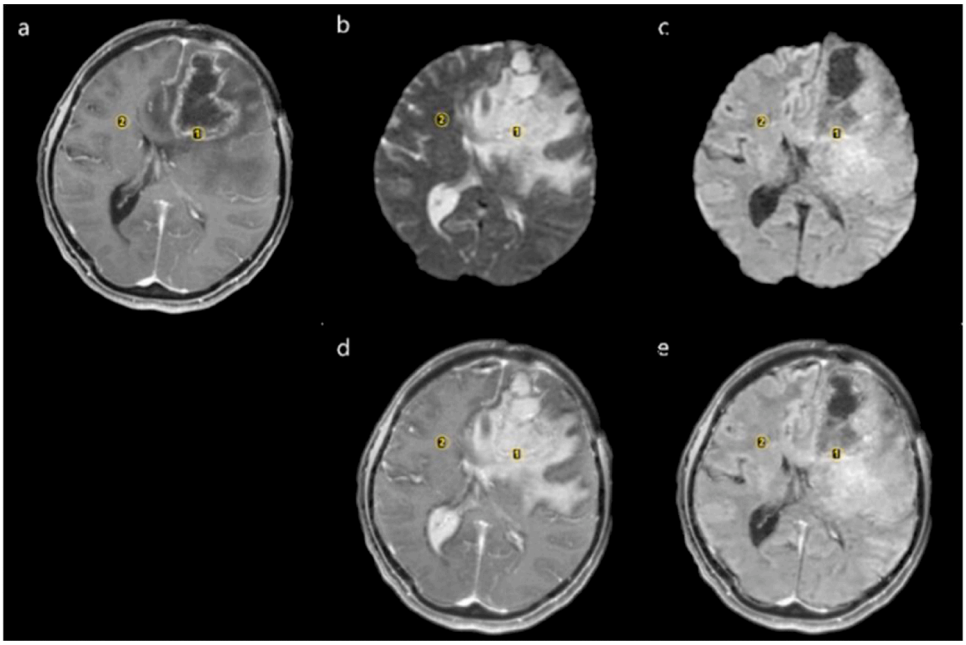

Fig. 5. image of a 54 year-old woman with grade IV glioma. (a) axial post-contrast T1-weighted (T1Gd) (b) diffusion-weighted image (DWI) with b-value 50 (b-50) (c) DWI with b-value 1000 (b-1000). (d) fused image of T1Gd + b50 with LRD fusion algorithm. (e)) fused image of T1Gd + b1000 with LRD fusion algorithm. In all images ROI 1 is enhancement region (ER) and ROI 2 is white matter region (WM).

as MRI. By developing the different MRI imaging protocols and high image contrast and resolution, MRI has become an important imaging modality for brain imaging. Many attempts have been made [17–19,21, 35–37] to differentiate the low-grade from high-grade gliomas with different MRI imaging protocols. However, there is still a need for improvement of MRI imaging accuracy for glioma grading. Image fusion is one solution for the improvement of diagnostic value for glioma grading.

The most striking results from Fig. 7 and Table 2 are that RSCs were increased with glioma grade. It may be assumed that RSCs increase with

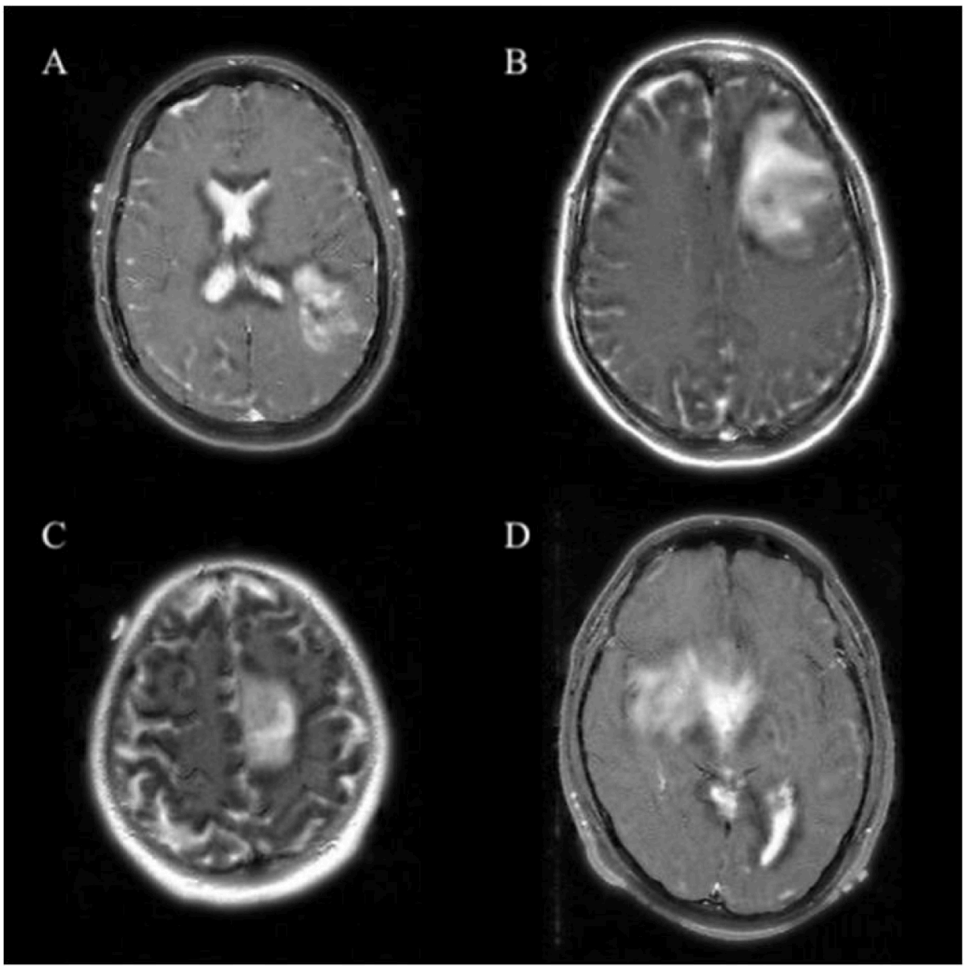

Fig. 6. examples of T1Gd fused images with b50 images with different glioma grade. (A) high-grade glioma (B), (c), and (D) low-grade glioma.

Table 2
The average RSCs for low-grade and high-grade gliomas.

	RSC_{T1Gd}	RSC_{b50}	RSC_{b500}	RSC_{b1000}	$RSC_{T1Gd+b50}$	$RSC_{T1Gd+b500}$	$RSC_{T1Gd+b1000}$
Low-grade	−0.155 ± 0.14	1.216 ± 0.238	0.851 ± 0.271	0.361 ± 0.26	0.339 ± 0.028	0.249 ± 0.051	0.219 ± 0.183
High-grade	0.702 ± 0.236	1.325 ± 0.733	0.783 ± 0.4	0.466 ± 0.38	0.924 ± 0.336	0.791 ± 0.217	0.739 ± 0.202
P-value	<0.001	0.744	0.714	0.55	<0.001	<0.001	0.002

glioma grade is related to the tumor cellularity and blood vessel proliferation of gliomas. Previous findings in the literature [9,10] highlighted the decrees of tumor cellularity with the increase of gliomas grade. Interestingly in the DWI images, tumors become brighter with decrees of tumor cellularity. This is in complete agreement with [9,38]. In the DWI images, the b-value determines the degree of diffusion weighting of DWI images. The higher b-value, the stronger the diffusion effects and image dephasing [39]. The result of dephasing is low signal intensity and image darkness. Therefore, an increase of b-value in DWI images may have led to RSCs decrease in DWI images shown in Table 2 and Fig. 7. This matches well with [40] and also confirms earlier studies [41,42]. As expected, our study shows that RSC_{T1Gd} increased with glioma grade because of increase blood vessel proliferation in high-grade glioma. This is in good agreement with Pope et al. [43].

No significant difference was observed between low-grade and high-grade gliomas in DWI (b50, b500, b1000) images (Table 2). This result corroborates previous results [42,44,45]. Curiously, this lack of significant relationship in DWI image is related to similar appearance and signal intensity of abscesses, edema, and tumor margin in the DWI image of low-grade and high-grade gliomas [45]. However, the statistical tests revealed that the RSCs between low-grade and high-grade gliomas in T1Gd and all fusion images (T1Gd + b50, T1Gd + b500, T1Gd + b1000) were significantly difference (Table 2), and we can use these images for the separation of low-grade from high-grade gliomas. Further analysis in RSCs curves showed that for low-grade and high-grade gliomas distinction, T1Gd images with cutoff value 0.0892 have the highest sensitivity, specificity, and AUC. Various studies have been suggested on T1 images, low-grade are often low signal intensity on T1 weighted images and T1 weighted with contrast enhancement, if present, is minimal [46]. However, high-grade gliomas on T1 weighted with contrast enhancement are high signal intensity. Therefore, this factor could well be responsible for differences of RSCs in T1Gd images and fusion images in low-grade and high-grade gliomas. We believed that because of tumor enhancement in T1 images in high-grade gliomas and rare enhancement in low-grade gliomas, T1Gd has the highest sensitivity, specificity, and AUC for differentiation of low-grade and high-grade gliomas. In addition, our results have several similarities with Pouratian et al. [47] findings.

Previous works [17,21] have failed to separate grade III and IV gliomas. The most conspicuous observation to emerge from Fig. 7 was, the

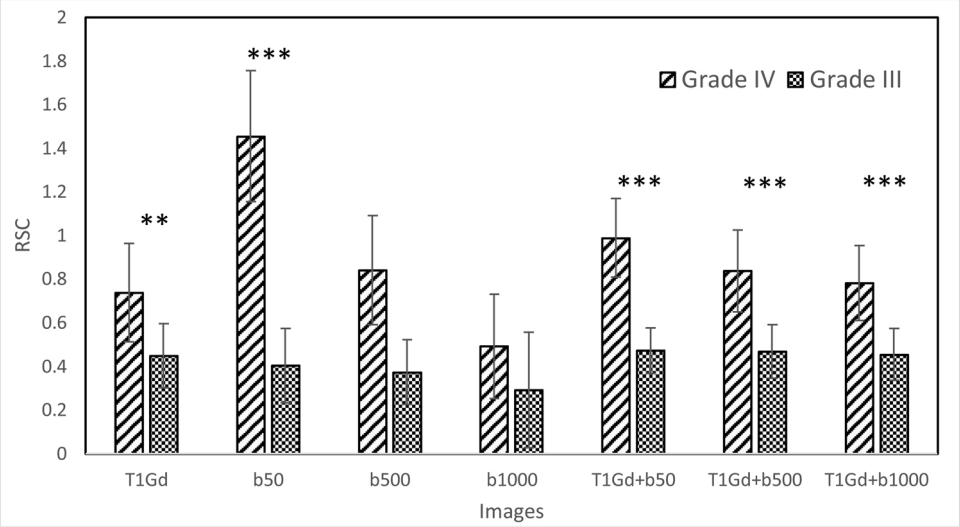

Fig. 7. Average RSCs of grade III and grade IV gliomas.
0* P-value<0.05 ** P-value <0.01 *** P-value<0.001.

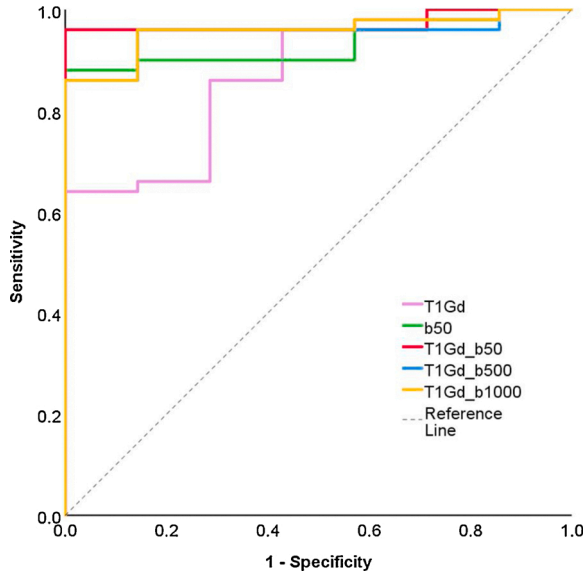

Fig. 8. ROC curve for differentiation of grade III and grade IV gliomas.

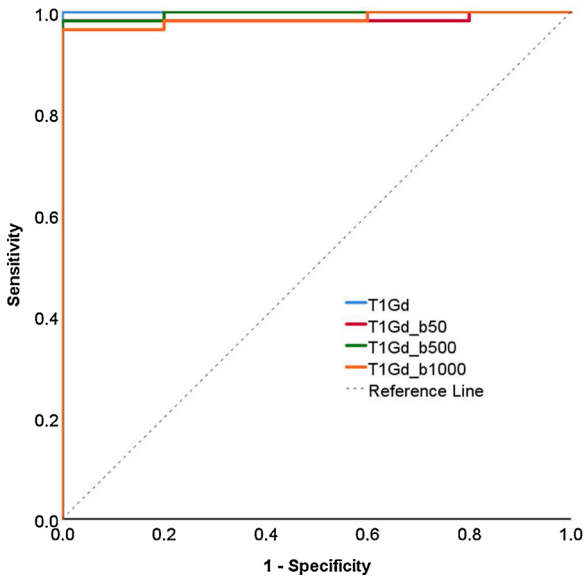

Fig. 9. ROC curve for differentiation of low-grade and high-grade gliomas.

Table 3
ROC parameters for differentiation of grade III and grade IV gliomas.

	RSC Cutoff value	AUC	Sensitivity	Specificity	Maximum Youden Index
T1Gd	0.6658	0.869	0.64	1	0.64
b50	0.6017	0.931	0.88	1	0.88
T1Gd + b50	0.6826	0.971	0.96	1	0.96
T1Gd + b500	0.7133	0.951	0.86	1	0.86
T1Gd + b1000	0.6886	0.957	0.86	1	0.86

average RSCs of grade IV gliomas were significantly higher than grade III in T1Gd, b50, and all fused images (T1Gd + b50, T1Gd + b500, T1Gd + b1000) (Fig. 5). Expectedly grater RSC, for grade IV gliomas in T1Gd images than grade III is related to more angiogenesis, blood vessel proliferation, and greater tumor blood vascular network in grade IV. The result of angiogenesis, tumor blood vascularization, and blood vessel proliferation is more tumor enhancement in T1Gd images and RSC increase. Our experiments are in line with previous results [19]. Interestingly for grade IV gliomas, RSCs were found greater than grade III in all fused images (Fig. 7). This correlation is related to the effect of the fusion algorithm because the resulting image contains information from both initial images.

The ROC curves analysis for differentiation of grade IV from grade III showed that using the LRD fusion algorithm was increased diagnostic values of fused images (Fig. 8, Table 3). For instance, in our study, the sensitivity, specificity, and AUC of T1Gd images for grade IV and III gliomas separation were calculated 0.64, 1, and 0.869, respectively. On the other hand, these values for b1000 DWI images were observed 0.5, 0.857, and 0.651, respectively. In this case, it was found that the use of LRD fusion algorithm can increase the sensitivity, specificity, and AUC of T1Gd + b1000 images for grade IV and III gliomas differentiation to 0.86 (72 % improvement toward b1000 images and 34.4 % improvement toward T1Gd images), 1 (16.6 % improvement toward b1000

images), and 0.957 (47 % improvement toward b1000 images and 10.12 % improvement toward T1Gd images) respectively. This finding highlights the usefulness of the LRD fusion algorithm as an appropriate method for grade IV and III gliomas differentiation.

We aware that our research may have limitations. A small sample size was chosen because of our study is a preliminary study and the main aim of this study is to examines the LRD medical image fusion algorithm usefulness into the clinical use. The most remarkable results to emerge from Fig. 7 and Table 3 for grade IV and III differentiation is that the sensitivity of the T1Gd is 0.64 and for b50 images is 0.88, and using the LRD fusion algorithm, the sensitivity has increased to 0.96 for T1Gd + b50 images. The reason for this increase in accuracy can be attributed to the combination of information in different images. T1Gd images provide information about the condition of blood vessels and blood vessel proliferation and tissue blood flow. On the other hand, DWI images provide information about the cellularity and motility of water molecules in the tissue. Finally, using the LRD fusion algorithm in the study, a single image can be created that includes information about vascular and tissue blood flow and cellularity, and the molecular motion of water in the tissue.

Notably, the LRD fusion algorithm increased the sensitivity, specificity, and AUC for differentiation of grade IV and grade III gliomas. In addition, it was found that the highest sensitivity, specificity, and AUC for grade IV and grade III differentiation belongs to T1Gd + b50. This finding highlights the usefulness of LRD fusion algorithms to increase the diagnostic value of the images.

5. Conclusion

The findings of this study indicate that for low-grade and high-grade gliomas delimitation, T1Gd images is a proper imaging protocol because of high sensitivity, high specificity, and availability in the most imaging department. Furthermore, our study provides considerable insight into using the LRD fusion algorithm for glioma grading by fusing the two different images with different data. Thus, we have found an innovative solution for grade III and IV gliomas differentiation. The evidence from this study suggests that we can use the LRD fusion algorithm to improve the diagnostic value of T1Gd and DWI images as the available MRI imaging protocol for grade III and IV gliomas differentiation. In summary, this paper has highlighted the importance of the LRD fusion algorithm as a method for grade III and IV gliomas differentiation.

Funding

This study was supported by Isfahan University of Medical Sciences, Isfahan, I.R. Iran [grant number 399077].

Ethics approval

The local research ethics committee (Isfahan university of medical sciences) has approved the study with ID: IR.MUI.MED.REC.1399.252.

CRediT authorship contribution statement

Amir Khorasani: Conceptualization, Methodology, Software, Data curation, Investigation, Methodology, Formal analysis, Visualization, Writing - original draft, Writing - review & editing. **Mohamad Bagher Tavakoli:** Funding acquisition, Supervision, Project administration, Investigation, Formal analysis, Visualization, Writing - original draft, Writing - review & editing. **Masih Saboori:** Investigation, Conceptualization, Visualization, Writing - original draft, Writing - review & editing. **Milad Jalilian:** Investigation, Methodology, Writing - original draft, Writing - review & editing.

Declaration of Competing Interest

The authors report no declarations of interest.

Acknowledgement

The authors thank Isfahan University of Medical Sciences for financial support of this work.

References

[1] C. Warmuth, M. Gunther, C. Zimmer, Quantification of blood flow in brain tumors: comparison of arterial spin labeling and dynamic susceptibility-weighted contrast-enhanced MR imaging, Radiology 228 (2) (2003) 523–532.
[2] B. Hakyemez, C. Erdogan, I. Ercan, N. Ergin, S. Uysal, S. Atahan, High-grade and low-grade gliomas: differentiation by using perfusion MR imaging, Clin. Radiol. 60 (4) (2005) 493–502.
[3] S. Sasaki, et al., Anaplastic pleomorphic xanthoastrocytoma associated with an H3G34 mutation: a case report with review of literature, Brain Tumor Pathol. 36 (4) (2019) 169–173.
[4] M. Law, et al., Low-grade gliomas: dynamic susceptibility-weighted contrast-enhanced perfusion MR imaging—prediction of patient clinical response, Radiology 238 (2) (2006) 658–667.
[5] H. Arvinda, et al., RETRACTED ARTICLE: glioma grading: sensitivity, specificity, positive and negative predictive values of diffusion and perfusion imaging, J. Neurooncol. 94 (1) (2009) 87–96.
[6] T. Hirai, et al., Prognostic value of perfusion MR imaging of high-grade astrocytomas: long-term follow-up study, Am. J. Neuroradiol. 29 (8) (2008) 1505–1510.
[7] N. Bulakbasi, M. Kocaoglu, A. Farzaliyev, C. Tayfun, T. Ucoz, I. Somuncu, Assessment of diagnostic accuracy of perfusion MR imaging in primary and metastatic solitary malignant brain tumors, Am. J. Neuroradiol. 26 (9) (2005) 2187–2199.
[8] N. Rollin, J. Guyotat, N. Streichenberger, J. Honnorat, V.-A.T. Minh, F. Cotton, Clinical relevance of diffusion and perfusion magnetic resonance imaging in assessing intra-axial brain tumors, Neuroradiology 48 (3) (2006) 150–159.
[9] N. Sadeghi, et al., Apparent diffusion coefficient and cerebral blood volume in brain gliomas: relation to tumor cell density and tumor microvessel density based on stereotactic biopsies, Am. J. Neuroradiol. 29 (3) (2008) 476–482.
[10] S. Cha, Update on brain tumor imaging: from anatomy to physiology, Am. J. Neuroradiol. 27 (3) (2006) 475–487.
[11] R.K. Gupta, et al., Relationships between choline magnetic resonance spectroscopy, apparent diffusion coefficient and quantitative histopathology in human glioma, J. Neurooncol. 50 (3) (2000) 215–226.
[12] S. Cha, E.A. Knopp, G. Johnson, S.G. Wetzel, A.W. Litt, D. Zagzag, Intracranial mass lesions: dynamic contrast-enhanced susceptibility-weighted echo-planar perfusion MR imaging, Radiology 223 (1) (2002) 11–29.
[13] J. Lee, S.H. Choi, J.H. Kim, C.H. Sohn, S. Lee, J. Jeong, Glioma grading using apparent diffusion coefficient map: application of histogram analysis based on automatic segmentation, NMR Biomed. 27 (9) (2014) 1046–1052.
[14] Y. Kang, et al., Gliomas: histogram analysis of apparent diffusion coefficient maps with standard-or high-b-value diffusion-weighted MR imaging—correlation with tumor grade, Radiology 261 (3) (2011) 882–890.
[15] Y. Bai, et al., Grading of gliomas by using monoexponential, biexponential, and stretched exponential diffusion-weighted MR imaging and diffusion kurtosis MR imaging, Radiology 278 (2) (2016) 496–504.
[16] P.-H. Lai, et al., Susceptibility-weighted imaging provides complementary value to diffusion-weighted imaging in the differentiation between pyogenic brain abscesses, necrotic glioblastomas, and necrotic metastatic brain tumors, Eur. J. Radiol. 117 (2019) 56–61.
[17] S.C. Jung, et al., Glioma: application of histogram analysis of pharmacokinetic parameters from T1-weighted dynamic contrast-enhanced MR imaging to tumor grading, Am. J. Neuroradiol. 35 (6) (2014) 1103–1110.
[18] G. Conte, et al., Comparison of T1 mapping and fixed T1 method for dynamic contrast-enhanced MRI perfusion in brain gliomas, Eur. Radiol. 29 (7) (2019) 3467–3479.
[19] K. Komatsu, et al., Arterial spin labeling method as a supplemental predictor to distinguish between high-and low-grade gliomas, World Neurosurg. 114 (2018) e495–e500.
[20] X.Z. Ma, et al., Application evaluation of DCE-MRI combined with quantitative analysis of DWI for the diagnosis of prostate cancer, Oncol. Lett. 17 (3) (2019) 3077–3084.
[21] A. Hilario, et al., The added value of apparent diffusion coefficient to cerebral blood volume in the preoperative grading of diffuse gliomas, Am. J. Neuroradiol. 33 (4) (2012) 701–707.
[22] J. Saini, et al., Differentiation of grade II/III and grade IV glioma by combining "T1 contrast-enhanced brain perfusion imaging" and susceptibility-weighted quantitative imaging,", Neuroradiology 60 (1) (2018) 43–50.
[23] M. Essig, et al., Perfusion MRI: the five most frequently asked technical questions, Am. J. Roentgenol. 200 (1) (2013) 24–34.
[24] A.G. Sorensen, Perfusion MR imaging: moving forward, Radiology 249 (2) (2008) 416–417.

[25] A. Villringer, et al., Dynamic imaging with lanthanide chelates in normal brain: contrast due to magnetic susceptibility effects, Magn. Reson. Med. 6 (2) (1988) 164–174.
[26] X. Li, X. Guo, P. Han, X. Wang, H. Li, T. Luo, Laplacian redecomposition for multimodal medical image fusion, IEEE Trans. Instrum. Meas. 69 (9) (2020) 6880–6890.
[27] G. Qi, J. Wang, Q. Zhang, F. Zeng, Z. Zhu, An integrated dictionary-learning entropy-based medical image fusion framework, Future Internet 9 (4) (2017) 61.
[28] K. Wang, G. Qi, Z. Zhu, Y. Chai, A novel geometric dictionary construction approach for sparse representation based image fusion, Entropy 19 (7) (2017) 306.
[29] Z. Zhu, Y. Chai, H. Yin, Y. Li, Z. Liu, A novel dictionary learning approach for multi-modality medical image fusion, Neurocomputing 214 (2016) 471–482.
[30] Z. Zhu, H. Yin, Y. Chai, Y. Li, G. Qi, A novel multi-modality image fusion method based on image decomposition and sparse representation, Inf. Sci. 432 (2018) 516–529.
[31] D.N. Louis, et al., The 2016 World Health Organization classification of tumors of the central nervous system: a summary, Acta Neuropathol. 131 (6) (2016) 803–820.
[32] M. Das, D. Gupta, P. Radeva, A.M. Bakde, NSST domain CT–MR neurological image fusion using optimised biologically inspired neural network, IET Image Process. 14 (16) (2020) 4291–4305.
[33] G. Wang, W. Li, Y. Huang, Medical image fusion based on hybrid three-layer decomposition model and nuclear norm, Comput. Biol. Med. 129 (2021) 104179.
[34] L.B. Rorke, Pathologic Diagnosis as the Gold Standard, ed, Wiley Online Library, 1997.
[35] A.M. Herneth, S. Guccione, M. Bednarski, Apparent diffusion coefficient: a quantitative parameter for in vivo tumor characterization, Eur. J. Radiol. 45 (3) (2003) 208–213.
[36] A.A.K.A. Razek, L. El-Serougy, M. Abdelsalam, G. Gaballa, M. Talaat, Differentiation of primary central nervous system lymphoma from glioblastoma: quantitative analysis using arterial spin labeling and diffusion tensor imaging, World Neurosurg. 123 (2019) e303–e309.
[37] Y.-b. Xi, et al., Differentiation of primary central nervous system lymphoma from high-grade glioma and brain metastasis using arterial spin labeling and dynamic contrast-enhanced magnetic resonance imaging, Eur. J. Radiol. 112 (2019) 59–64.
[38] L. Tang, X.J. Zhou, Diffusion MRI of cancer: from low to high b-values, J. Magn. Reson. Imaging 49 (1) (2019) 23–40.
[39] J.H. Burdette, D.D. Durden, A.D. Elster, Y.-F. Yen, High b-value diffusion-weighted MRI of normal brain, J. Comput. Assist. Tomogr. 25 (4) (2001) 515–519.
[40] Ó. Peña-Nogales, D. Hernando, S. Aja-Fernández, R. de Luis-Garcia, Determination of optimized set of b-values for apparent diffusion coefficient mapping in liver diffusion-weighted MRI, J. Magn. Reson. 310 (2020) 106634.
[41] L. Minati, W.P. Węglarz, Physical foundations, models, and methods of diffusion magnetic resonance imaging of the brain: a review, Concepts Magn. Reson. A: Bridg. Educ. Res. 30 (5) (2007) 278–307.
[42] P.W. Schaefer, P.E. Grant, R.G. Gonzalez, Diffusion-weighted MR imaging of the brain, Radiology 217 (2) (2000) 331–345.
[43] W.B. Pope, G. Brandal, Conventional and advanced magnetic resonance imaging in patients with high-grade glioma, Q. J. Nucl. Med. Mol. Imaging 62 (3) (2018) 239.
[44] J.A. Brunberg, et al., In vivo MR determination of water diffusion coefficients and diffusion anisotropy: correlation with structural alteration in gliomas of the cerebral hemispheres, Am. J. Neuroradiol. 16 (2) (1995) 361–371.
[45] L.C.H. da Cruz Jr, E.L. Gasparetto, R.C. Domingues, R.C. Domingues, Diffusion-weighted MR imaging in brain tumor, MAGNETOM Flash 2 (2008) 21–29.
[46] A. Pirzkall, et al., Metabolic imaging of low-grade gliomas with three-dimensional magnetic resonance spectroscopy, Int. J. Radiat. Oncol. Biol. Phys. 53 (5) (2002) 1254–1264.
[47] N. Pouratian, A. Asthagiri, J. Jagannathan, M.E. Shaffrey, D. Schiff, Surgery Insight: the role of surgery in the management of low-grade gliomas, Nat. Clin. Pract. Neurol. 3 (11) (2007) 628–639.